Front. Environ. Sci. Eng. 2022, 16(11): 147
https://doi.org/10.1007/s11783-022-1582-z

RESEARCH ARTICLE

Combination of steam-enhanced extraction and electrical resistance heating for efficient remediation of perchloroethylene-contaminated soil: Coupling merits and energy consumption

Rui Yue[1], Zhikang Chen[1], Liujun Liu[1], Lipu Yin[2], Yicheng Qiu[1], Xianhui Wang[1], Zhicheng Wang[1], Xuhui Mao (✉)[1]

1 School of Resource and Environmental Sciences, Wuhan University, Wuhan 430079, China
2 China State Science Dingshi Environmental Engineering Company, Beijing 100020, China

HIGHLIGHTS

- Coupling merits of SEE and ERH were explored by a laboratory-scale device.
- SEE promotes the soil electrical conductivity and ERH process.
- Preheating soil by ERH improves the soil permeability and SEE.
- Combined method is more energy-efficient for perchloroethylene extraction.

GRAPHIC ABSTRACT

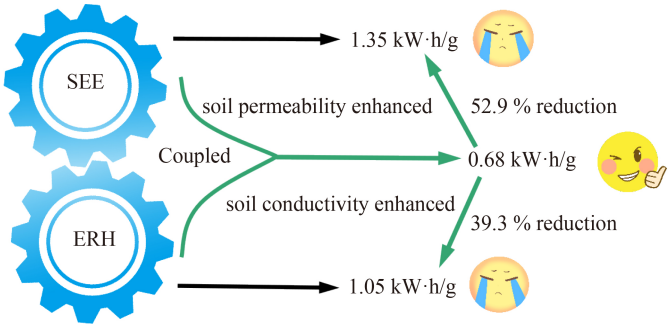

ARTICLE INFO

Article history:
Received 13 February 2022
Revised 18 April 2022
Accepted 25 April 2022
Available online 10 June 2022

Keywords:
Steam-enhanced extraction
Electrical resistance heating
Dense nonaqueous phase liquid
Soil remediation
Energy consumption

ABSTRACT

In situ thermal desorption (ISTD) technology effectively remediates soil contaminated by dense nonaqueous phase liquids (DNAPLs). However, more efforts are required to minimize the energy consumption of ISTD technology. This study developed a laboratory-scale experimental device to explore the coupling merits of two traditional desorption technologies: steam-enhanced extraction (SEE) and electrical resistance heating (ERH). The results showed that injecting high-density steam (> 1 g/min) into loam or clay with relatively high moisture content (> 13.3%) could fracture the soil matrix and lead to the occurrence of the preferential flow of steam. For ERH alone, the electrical resistance and soil moisture loss were critical factors influencing heating power. When ERH and SEE were combined, preheating soil by ERH could increase soil permeability, effectively alleviating the problem of preferential flow of SEE. Meanwhile, steam injection heated the soil and provided moisture for maintaining soil electrical conductivity, thereby ensuring power stability in the ERH process. Compared with ERH alone (8 V/cm) and SEE alone (1 g/min steam), the energy consumption of combined method in remediating perchloroethylene-contaminated soil was reduced by 39.3% and 52.9%, respectively. These findings indicate that the combined method is more favorable than ERH or SEE alone for remediating DNAPL-contaminated subsurfaces when considering ISTD technology.

1 Introduction

Subsurfaces contaminated by dense nonaqueous phase liquids (DNAPLs), such as chlorinated solvents and coal tar, present significant technical and economic challenges in the environmental remediation field (Zhang et al., 2019; Geng et al., 2021). DNAPLs typically exist as a stable pool above a low-permeability zone due to capillary

✉ Corresponding author
E-mail: clab@whu.edu.cn

force (Geng et al., 2021). Several factors make DNAPL remediation very challenging, including their low limits for risk screening, low aqueous solubility, and vertical mobility (Martin et al., 2016). *In situ* thermal desorption (ISTD) has been increasingly used in site remediation in the last two decades because it can quickly treat DNAPL source regions. For example, the performance of ISTD is less hampered by geological stratification and mass transfer resistances that limit other *in situ* remediation techniques (e.g., *in situ* chemical oxidation, *in situ* soil stabilization, and *in situ* flushing remediation) (Triplett Kingston et al., 2010). ISTD technology heats the soil to create physical conditions that promote the volatilization of pollutants (Horst et al., 2021). According to the mode of heating, the main ISTD technologies include steam-enhanced extraction (SEE), electrical resistance heating (ERH), thermal conductive heating, and radiofrequency heating (Triplett Kingston et al., 2010). Although full-scale applications of various ISTD technologies have been reported, more efforts are still required to alleviate their common problem of relatively high-energy consumption.

Among these ISTD technologies, both SEE and ERH are low-temperature (~100 °C) thermal technologies that are more environmentally friendly for soil. The SEE method introduces steam into subsurfaces to create a thermodynamic driving force, moving contaminants toward the central extraction well (USEPA, 2004). Generally, soil hydraulic conductivity should be higher than 10^{-5} cm/s for steam penetration (Trine et al., 2019). SEE can be used to recover volatile organic compounds (VOCs) and semi-VOCs from unsaturated and saturated zones using two main removal mechanisms: (a) physical displacement of contaminants (the contamination is mobilized by hydrodynamic forces and the reduction in viscosity and interfacial tension); (b) vaporization and extraction as a vapor phase (steam distillation and volatilization of contaminants) (Sleep and McClure, 2001; Tse et al., 2001; Tzovolou et al., 2011; Trine et al., 2019). One of the limitations of steam injection is the gravity-assisted downward movement of nonaqueous phase liquids (NAPLs) that accumulate in the condensation front (Kaslusky and Udell, 2005; Peng et al., 2013). Therefore, sufficient steam is required to develop a uniform steam zone below the NAPL zone to prevent the downward movement of NAPLs. Besides, increasing the steam injection rate could address the problem of steam override caused by the lower density of steam relative to liquids (Davis, 1998). The effectiveness of the frontal displacement is weakened when steam override occurs, which reduces the vertical sweep efficiency of the steam displacement process (Davis, 1998). However, the pressure of the injected steam is limited by the soil overburden pressure. The fracturing of soil can occur when the steam pressure is higher than the soil overburden pressure. Steam is ineffective for removing contaminants trapped in the porous matrix because it flows through permeable fractures (Davis, 1998; Stephenson et al., 2006). Therefore, selecting an appropriate injection pressure to improve steam penetration in the soil is critical for improving the heating efficiency of SEE.

ERH delivers electric current to subsurfaces, and the natural resistance of subsurfaces to the flow of electrical current heats the entire treatment area based on Joule's Law (Ding et al., 2019). As subsurfaces are heated, contaminants are volatilized (Heron et al., 1998). The heating efficiency of ERH is affected by the applied electric field strength and subsurface properties (Han et al., 2020). The applied electric field strength can be artificially regulated by adjusting the voltage and the spacing between electrode wells. However, the electric field strength during full-scale applications is limited by the safe working voltage and drilling cost of wells (USEPA, 2004). Meanwhile, factors influencing subsurface properties are very complex. For example, soil electrical conductivity is significantly affected by soil moisture. The presence of a large volume of pore fluid results in the thermal loss of ERH, whereas low moisture content decreases the electrical conductivity of the soil. Previous studies demonstrated that the complexity of subsurfaces leads to uncertainty in achieving decontamination when ERH is used (Martin and Kueper, 2011; Munholland, 2015; Munholland et al., 2016). A lingering problem of ERH is uneven subsurface heating because of the large heating rate difference between the near-electrode region and the center of the electrode array (Carrigan and Nitao, 2000). As the spatial electric power density of electrodes decreases, soils around these electrodes receive significantly more heat energy (Li et al., 2020). This problem also leads to the fastest evaporation of water around these electrodes, necessitating constant replenishment to maintain good electrical conductivity of the soil around these electrodes.

The combination of SEE and ERH technologies can improve thermal desorption efficiency, benefitting from the advantages of both methods. For example, SEE is suitable for high-permeability soil, whereas ERH is suitable for many soil types. So far, two full-scale site remediation cases have been reported that are implementing a combination of SEE and ERH technologies. The first remedy was performed at the Lawrence Livermore National Laboratory gasoline spill site (Newmark and Aines, 1995). During the 21-week operation, the combined method removed more than 7600 gallons of gasoline trapped in the soil, outperforming expectations due to the previous significant difficulty in accomplishing the same goal experienced using other decontamination methods (Newmark and Aines, 1995). The second remedy case that combined SEE and ERH was implemented at the Young–Rainey STAR Center (Heron et al., 2005). In this process, SEE and ERH were used to heat both high- and low-permeability zones, resulting in very effective and uniform heating. After 4.5 months of operation, the sampling process achieved high remedial efficiency of 99.99% for volatile contaminants. Although the two site cases yielded high thermal desorption efficiency for volatile organics, their coupling

benefits relative to individual technology were still unclear. In addition, few studies have been conducted to elucidate the benefits of the combined process at a laboratory scale. Therefore, in this study, an experimental device combining SEE and ERH ("SEE+ERH") is developed to investigate the characteristics of the heating process, influencing factors, and energy utilization efficiencies of the combined method. The laboratory-scale device has the advantage of easily monitoring various parameters, allowing an accurate evaluation of the temperature change and desorption efficiency. Chlorinated solvent perchloroethylene (PCE) was chosen as the targeted pollutant. We hope that the findings of this study will aid in understanding the spatial and temporal variation of a thermal field of this combined process, thereby providing clues to its optimization in futures engineering practice.

2 Materials and methods

2.1 Chemicals and materials

PCE and hexane (GC grade) were purchased from the Aladdin Chemical Reagent, China. Sodium sulfate (Na_2SO_4), 98% sulfuric acid (H_2SO_4), and other chemicals were purchased from the Sinopharm Chemical Reagent, China. Millipore-Q water with a resistivity of 18.2 MΩ/cm was used throughout the experiments. Silica sand, loam, and clay were obtained from the Songyu company in Suzhou, China. The soils were ground into small particles and sieved through 100-mesh screens. Table S1 shows the basic physical properties of the soil samples in the supplementary materials (SM).

2.2 Experimental setup and procedures

Fig. 1 shows the schematic illustration of the "SEE+ERH" laboratory setup. The setup consisted of a steam injection part, ERH equipment, soil column, and monitoring unit. For the steam injection part, a metering pump delivered the desired water flow rate to a steam generator. Steam from the generator was injected from the top of the soil column to produce a vertical downward flow through the column. Stainless steel-connecting pipes were wrapped with heater tape to ensure the steam temperature before injection. A voltage-adjustable transformer was used to provide AC electrical power for ERH. The transformer was connected to a standard power grid (AC phase voltage, 220 V, and 60 Hz). The soil column was made of polytetrafluoroethylene, with an inner diameter of 5 cm, an outer diameter of 6 cm, and a length of 15 cm. A 300-mesh screen was placed at the bottom of the soil column when the soil sample was packed. The top of the packed soil was 2 cm lower than the steam injection point. It allowed the uniform distribution of steam when it was injected. Two electrodes were installed symmetrically on the inner wall of the soil column. The electrode was made of a stainless steel sheet, with a width of 1.5 cm and a length of 12 cm. Off-gas from the soil column went through a water condenser. The condensed liquid was collected into a round-bottom flask, whereas the gas was introduced to a VOC detector. Three thermocouples were inserted in the

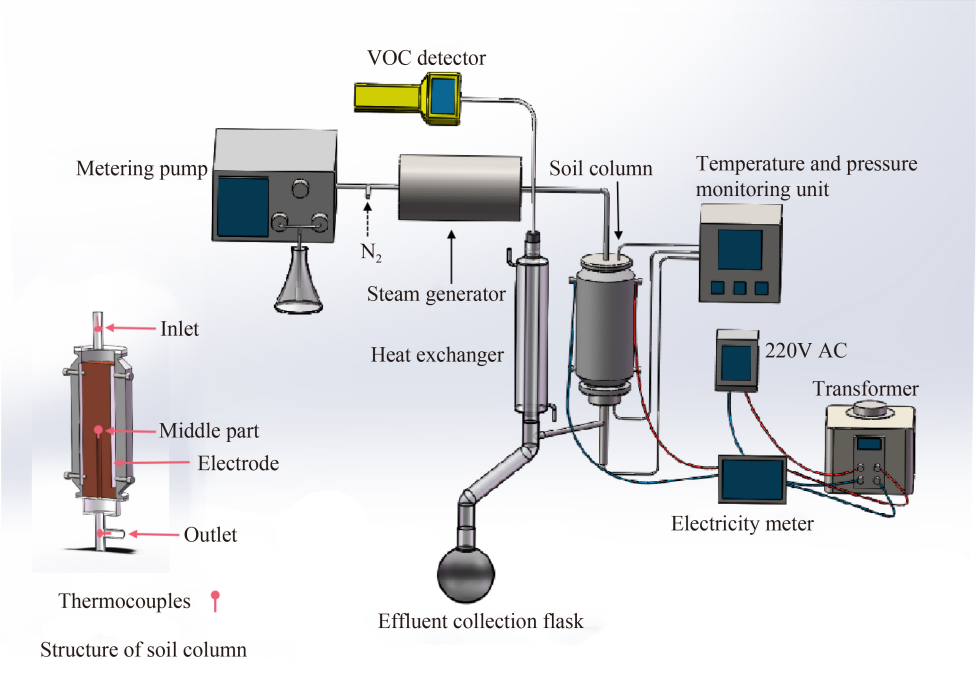

Fig. 1 Schematic of laboratory-scale "SEE+ERH" experimental device.

column's top, middle, and bottom parts, respectively, to monitor temperature (see the detailed column structure shown in Fig. 1). An electricity meter was connected to the transformer to monitor AC voltage, power, and electrical current. Two pressure gauges were set at the top and bottom of the column to monitor pressure. For the experiments exploring PCE removal, nitrogen gas (100 mL/min) was purged. A portable VOC detector (ppb RAE 3000) monitored the PCE concentration change in the off-gas. The VOC detector had a built-in sampling pump with a 500 mL/min extraction rate. A schematic of the actual laboratory-scale "SEE+ERH" device is shown in Fig. S1 in SM.

A 300-g dry soil sample was mixed with water to achieve a given moisture content to investigate the temperature profiles of the soil column during heating. Afterward, the soil was packed into the column. For PCE-contaminated soil preparation, 0.2-mL PCE was uniformly dropped into the 300-g soil with a moisture content of 20%, and then the mixture was uniformly stirred and aged for 24 h in a sealed glass bottle. Considering the volatility of PCE, the initial PCE concentration was determined only when the contaminated soil was packed. For the PCE removal experiments, the heating process was terminated when the VOC concentration stabilized under 36.83 mg/m^3 (5 ppm) in the off-gas. After the soil column cooled to room temperature, ~3-g soil samples were taken from the bottom of the soil column for analysis.

2.3 Analytical methods

After the experiments, the soil samples from the bottom of the column were used to analyze the residual PCE concentration. A gas chromatograph (GC; 2014C model, Shimadzu) equipped with a flame ionization detector and a capillary column (DB-FFAP, 30 m × 0.32 mm, 0.25 μm) was used to quantify the PCE concentration in the samples. 3-g soil samples were first added to 5 mL of 1-mol/L H_2SO_4 and extracted using 10-mL hexane in a 20-mL sealed vial on a reciprocating shaker for 24 h. After 6 h of standing, 1-μL hexane extract (upper liquid) was transferred to 10-μL GC syringes for GC detection. For the PCE in an aqueous phase, the aqueous sample (2.0 mL) from the collection flask was extracted with hexane (1.0 mL) for 10 min on a shaker and stood for 5 min for separation in a 20-mL sealed vial; then 0.1-g Na_2SO_4 was added to the vial. 1-μL hexane extract was transferred to a 10-μL GC for GC detection.

Steam quality (x) is defined as the proportion of pure steam in the vapor phase. If liquid water is not present, the steam quality is 100%. Steam quality (x) from the steam generator was detected using a tracer method (Fournier et al., 2009). Water will evaporate at high temperatures, and water droplets in the steam will dissolve chloride ions. Chlorine ion concentrations of the initial water C_{initial} and the condensed water $C_{\text{condensed}}$ at the steam generator outlet were detected, respectively. The chlorine ion concentration was determined by ion chromatography (Metrohm). Steam quality (x) can be calculated using Eq. (1):

$$x = (C_{\text{initial}} - C_{\text{condensed}})/C_{\text{initial}}. \quad (1)$$

2.4 Energy consumption for PCE desorption

The mass of recovered PCE (M) is composed of the part in the off-gas (M_1), which is obtained by integrating the PCE concentration in the off-gas, and the part in the condensed liquid (M_2). The mass of recovered PCE (M) is calculated using Eqs. (2)–(4):

$$M = M_1 + M_2, \quad (2)$$

$$M_1 = \int_0^t V_1 C_1 t = V_1 \int_0^t C_1 t, \quad (3)$$

$$M_2 = V_2 C_2, \quad (4)$$

where V_1 represents the extraction rate of 500 mL/min; C_1 represents the PCE concentration in the off-gas; t represents the desorption time; V_2 represents the volume of condensed liquid; C_2 represents the PCE concentration in the condensed liquid. The value of $\int_0^t C_1 t$ *is* obtained by calculating the area enclosed by the PCE concentration curve and the X-axis of time. Energy consumption (Q) of the combined method for PCE removal only considers the energy input for heating, namely, the energy for steam generation (Q_s) and electrical heating by the electrical field (Q_e) (see Eq. (5)).

$$Q = Q_s + Q_e, \quad (5)$$

$$Q_s = mc(T_1 - T_2) + m\Delta hx, \quad (6)$$

where m represents the total mass of water used to produce steam during SEE. T_1 represents the temperature of boiling point (100 °C) at one atmosphere. T_2 represents the initial temperature of water (25 °C in this study); c represents the specific heat capacity of water. Δh represents the latent heat, and x represents the steam quality (90% in this study). Notably, small amounts of energy for injecting steam (i.e., the increased steam heat value after 100 °C) were excluded when calculating Q_s. In other words, the energy required for the metering pump and nitrogen gas purging was not considered. Q_e was directly calculated using the electricity meter. Energy utilization efficiency (kW·h/g) for PCE desorption was calculated by energy consumption (Q) divided by the mass of the recovered PCE (M).

3 Results and discussion

3.1 Heating soil by SEE

The injection rate is an important parameter for a steam injection process. As shown in Fig. 2, as the steam injection rate increased, the temperature at the middle part and the outlet increased. For a steam injection rate of 0.5 g/min, after 3 h, the temperature in the middle of the column increased to ~84 °C for all soil moisture contents (Fig. 2a–2c), indicating that steam could barely penetrate

the soil column at a low steam injection rate. Because of the low permeability of the soil, a low steam injection rate (pressure) may be unable to overcome the total capillary pressure required for water displacement (Tzovolou et al., 2011). For a steam injection rate of 1 g/min (Fig. 2d–2f), the initial soil moisture content significantly affected the increase in temperature of the soil. At an initial soil moisture content of 10% (Fig. 2d), the middle and outlet of the column reached 100 °C after 30 and 60 min, respectively, indicating that steam evenly penetrated the soil column. However, at a soil moisture content of 13.3% (Fig. 2e), the rate of temperature increase in the middle of the soil column decreased; meanwhile, the temperature of the outlet reached 100 °C earlier than that of the middle, indicating that steam did not evenly penetrate the soil column. It means that preferential flows of steam occurred. Steam flowed through the middle part via routes other than the thermocouple. This phenomenon was more obvious when the initial moisture raised to 16.7% (Fig. 2f) or the steam injection rate increased to 1.5 g/min (Fig. 2g–i).

When the steam pressure is greater than the overburden pressure of soil, the fracturing of the soil may occur, which may result in preferential flows of steam. Assume that the flow of steam and water in the soil obeys Darcy's law (Eq. (7)) (Brouwers and Gilding, 2006),

$$\nabla p = -\frac{\mu}{\alpha}\vec{v}, \tag{7}$$

where ∇p represents the fluid pressure difference, $\vec{v}$ represents the fluid velocity, μ represents permeability coefficient, and α represents the fluid viscosity. The steam injection rate ($\vec{v}$) is positively related to the steam pressure. Therefore, the increased injection rate of steam could accelerate soil fracturing. On the other hand, the high moisture content may significantly reduce the relative permeability of steam and prevent the convective flow, which in turn increases steam pressure under a constant steam injection rate. As shown in the following Corey relations (Eq. (8)) (Piquemal, 1994), the relative permeability of gas K_G will decrease with increasing water saturation S.

$$K_G = (1 - S_e^2)(1 - S_e)^2 \tag{8}$$

The effective saturation of the wetting fluid S_e is defined as

$$S_e = (S - S_i)/(1 - S_i) \tag{9}$$

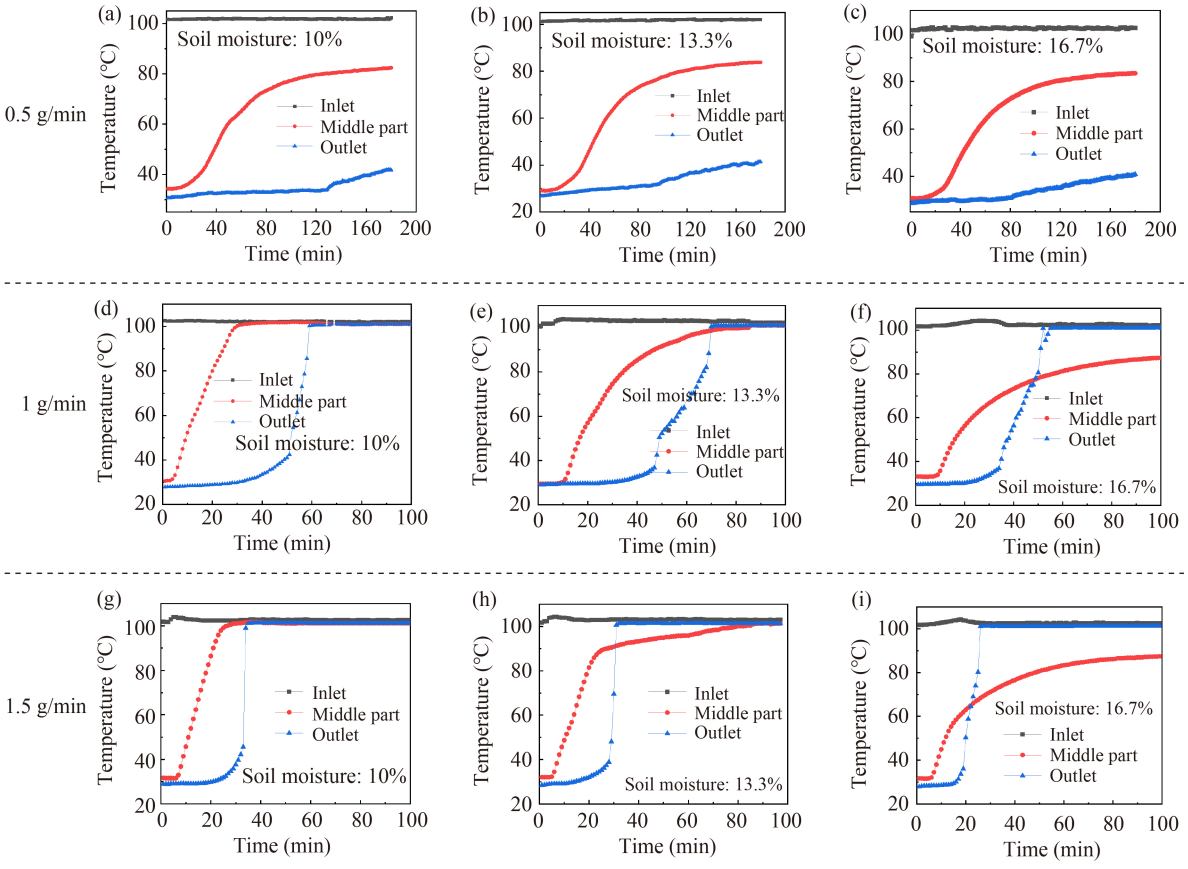

Fig. 2 Temperature profiles of the inlet, middle, and outlet parts of the soil column with a steam injection rate at 0.5 g/min (a–c), 1 g/min (d–f), and 1.5 g/min (g–i). For each steam injection group, loam soil samples with moisture contents of 10%, 13.3%, and 16.7% were tested.

where S_i represents the irreducible saturation of the wetting fluid. As shown in Fig. S2 in SM, cracks in the soil become more obvious as the soil moisture increases. Dimitra et al. reported that steam injected in a low-permeable soil gradually increased water saturation, preventing the steam flow and changing the pore structure of the soil with the creation of micro-fractures (Tzovolou et al., 2011). Therefore, under the conditions of high soil moisture content and high steam injection rate, SEE could suffer from the problem of preferential steam flows.

To further investigate the effect of soil permeability on the occurrence of steam overburden, we compared three types of soils with varying permeability levels. As shown in Fig. 3a–3c, for the sandy soil, the middle part of the column reached 100 °C faster than the outlet, even when the steam injection rate increased to 2 g/min, indicating that preferential pathways for steam migration did not occur in the sand. For both loam (Fig. 3d–3f) and clay (Fig. 3g–3i), the problem of preferential steam flows became more severe with increasing steam injection rates. Notably, the preferential steam flows in clay required a higher injection rate than in loam, implying that clay had a higher overburden pressure than loam. In addition, compared with loam, the temperature and pressure of the inlet of the clay-packed column increased to a relatively higher value. Especially at an injection rate of 1.5 g/min (Fig. S3a), the temperature and pressure of the inlet increased to 108 °C and 0.3 kPa, respectively, and further raised to 115 °C and 0.5 kPa, respectively, at an injection rate of 2 g/min (Fig. S3b).

Injecting steam into fractured media cannot uniformly heat the entire soil, making it ineffective at displacing contaminants trapped in the porous matrix (Davis, 1998). Therefore, it is important to control the steam injection rate and increase soil permeability to prevent the generation of preferential pathways. As shown in Fig. S4 in SM, we presented two ways of steam transport in the soil matrix: a) homogeneous steam transport in the void of soil under pressure driving; b) steam transport dominated by flows in preferential pathways as occur fracturing occurs. The steam flow by preferential pathways should be avoided to maximize the thermal desorption efficiency of steam.

3.2 Heating soil by ERH

The effects of soil moisture and electric field strength on ERH are investigated. Both the temperature rising rate

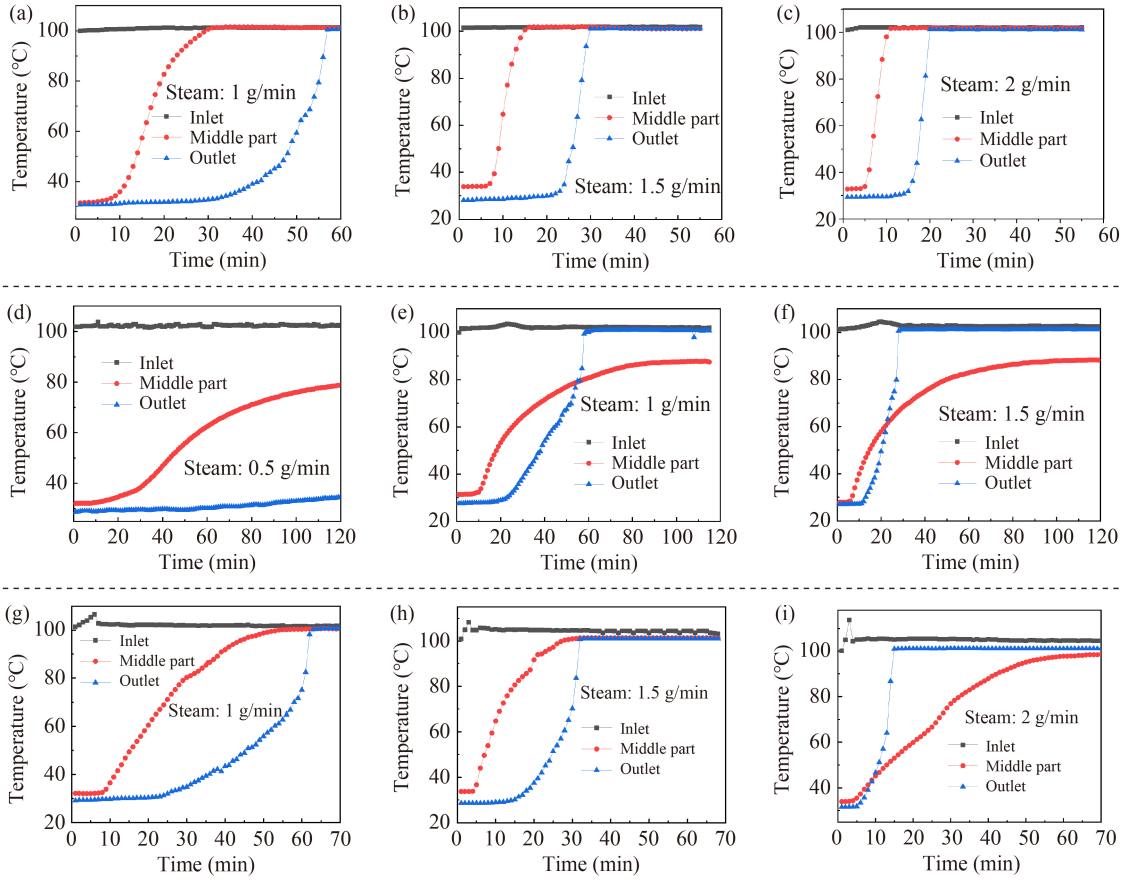

Fig. 3 Temperature profiles of the inlet, middle part, and outlet of the soil column when steam was injected into different media: sand (a–c), loam (d–f), and clay (g–i). Initial soil moisture was set at 20% for all tested samples.

(Fig. 4a–4c) and heating power (Fig. 4d–4f) increased with increasing soil moisture content. When soil moisture was 10%, even under 16 V/cm (Fig. 4c), the soil could not be heated to the boiling point of water because of the low heating power, implying that ERH required sufficient water to provide sufficient electrical conductivity. In addition, low moisture content also caused uneven soil heating. As shown in Fig. 5, when the soil moisture content was 10%, the soil temperature close to the electrode was significantly higher than that in the middle part of the column. As the soil moisture increased, the difference in soil temperature profile gradually decreased. The profiles indicate that soil moisture content of 26.7% ensured the quickest temperature rise rate for all levels of electric field strength. In addition, note that the electric field strength significantly accelerated the temperature rise rate. The temperature of soil with 30% moisture content raised to 94 °C after 4 h of heating at 8 V/cm (Fig. 4a); meanwhile, the soil could reach 100 °C within 60 and 25 min at 12 and 16 V/cm, respectively (Fig. 4b and 4c).

The electric conductivity and electric field strength of soil determine the electrical current across the soil matrix, thereby influencing the heating rate of soil (Han et al., 2020). Soil electrical conductivity (σ) is affected by different factors, such as soil porosity, soil moisture content, soil temperature, and electrical conductivity of pore fluid (Archie, 1942; Arps, 1953; Cai et al., 2017). The influence of the above factors on σ can be expressed using the following equations:

$$\sigma_s = \theta^m S_w^n \sigma_w, \tag{10}$$

$$\sigma_{w2} = \sigma_{w1} \frac{T_2 + 21.5}{T_1 + 21.5}, \tag{11}$$

where σ_s and σ_w denote the volume conductivity of the porous medium and the conductivity of the pore fluid, respectively. θ denotes porosity; S_w represents the water saturation of the medium; m and n represent cementation and saturation indexes, respectively; σ_{w1} denotes water conductivity at the reference temperature T_1; σ_{w2} denotes water conductivity when the temperature rises to T_2. According to Eq. (10), when soil moisture content increased, soil electrical conductivity increased, increasing ERH efficiency. Fig. 4d–4f depict how soil moisture influences soil conductivity and, thus, the power of ERH. In the initial stage of ERH, the heating power increased with increasing soil moisture content. Subsequently, heating power plateaus were found at 8 V/cm, and heating power peaks appeared for most 12 and 16 V/cm trials. When ERH was initialized, the heating power rapidly increased, and soil temperature was elevated accordingly. In turn, the temperature increase decreased the viscosity of the pore water of soil, increasing soil electrical conductivity (see Eq. (11)) and accelerating the power rise. When the soil temperature reached the boiling point of water, e.g., 60 min for 12 V/cm, the electrical conductivity of soil no longer increased with increasing temperature but instead decreased because of the rapid evaporation of water. Therefore, the variation of heating power can be used as an important and readily available indicator for judging

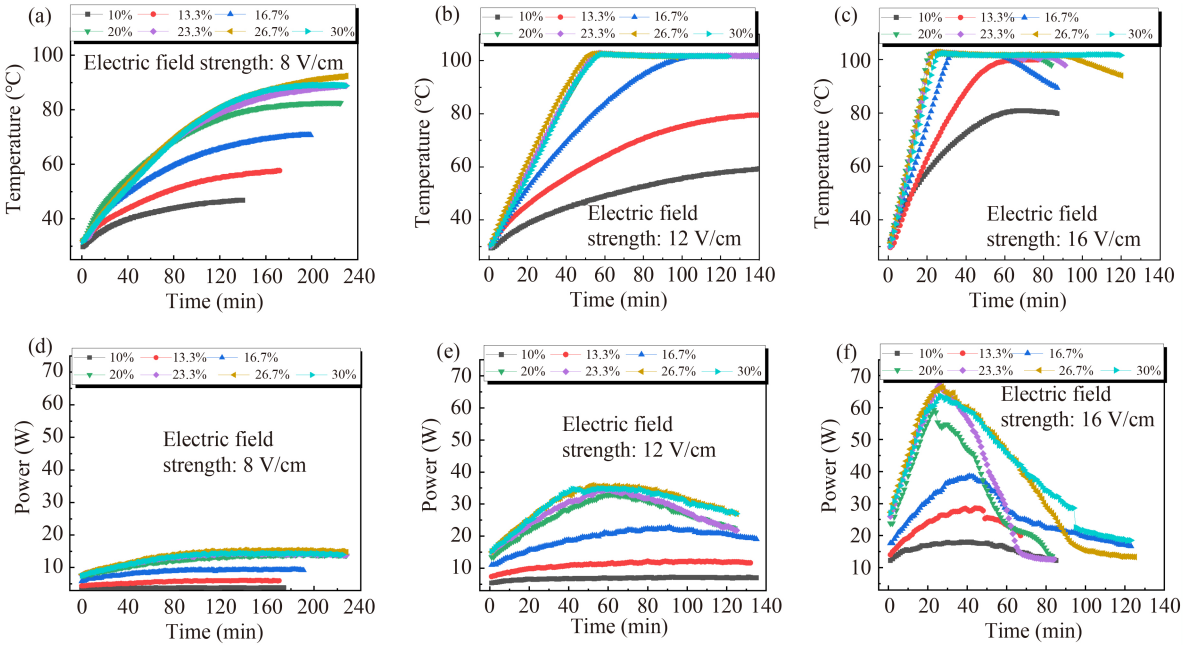

Fig. 4 Profiles of soil temperature (middle part of the column) and heating power for the electrical resistance heating of loam sample at 8 V/cm (a, d), 12 V/cm (b, e), 16 V/cm (c, f). The sample moisture content ranged from 10% to 30%.

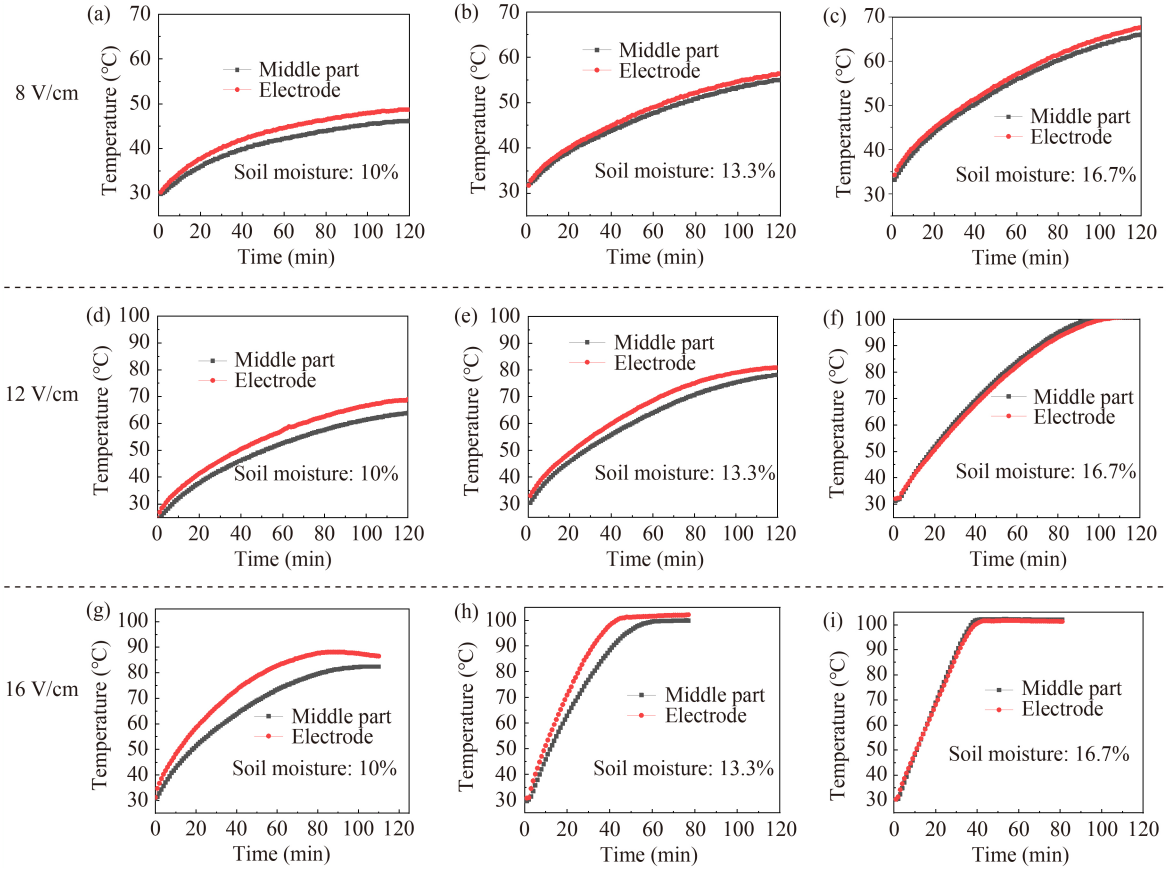

Fig. 5 Temperature profiles of the middle part of the soil column and electrodes. The temperature of the electrode was measured by inserting a thermocouple close to the electrode (~3-mm spacing).

soil moisture state. The time point showing the electrical power peak is the right moment for moisture adjustment.

3.3 Heating soil by the combination of SEE and ERH

Fig. 6a depicts the combination of ERH (8 V/cm) and SEE (0.5 g/min) for the heating of soil. Steam penetrated the entire soil column within 100 min, showing a significantly higher temperature rise rate than SEE alone. At a low steam injection rate of 0.5 g/min, steam barely penetrated the soil column (see Fig. 2a), whereas this was not observed for the combined method, suggesting that ERH could reduce the resistance of steam transport in soil. In addition, the heating power of ERH reached a stable value of approximately 17 W within 65 min, and the power did not exhibit the same peak value as that shown in Fig. 4 even though 100 °C was achieved for the soil matrix. Fig. 6b shows the temperature profile of soil

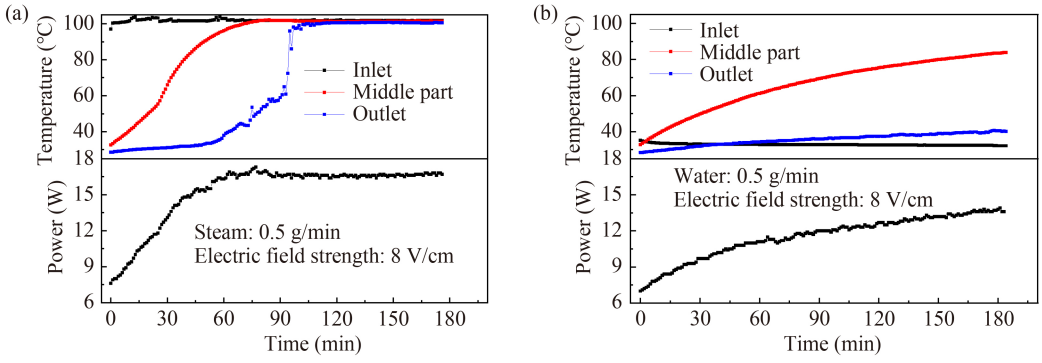

Fig. 6 (a) Profiles of temperature and heating power when loam soil was heated by ERH (8 V/cm) and SEE in combination; (b) profiles of temperature and heating power by ERH (8 V/cm) while the same amount of water was injected. The initial soil moisture was set at 20%. Both steam and water were injected at a rate of 0.5 g/min.

and heating power for ERH alone, with the injection of room-temperature water at a 0.5-g/min rate. After 180 min, the soil temperature and electrical power were only increased to 84 °C and 14 W. Adding water yielded a lower heating efficiency than the steam injection, suggesting that the moisture from the SEE process could accelerate the temperature rise rate and avoid the decrease in power through continuous moisture supply.

Fig. 7a shows the temperature profile when steam was injected at a higher rate of 1 g/min. When both SEE (1 g/min) and ERH were initialized simultaneously, the outlet of the column reached 100 °C faster than the middle part. Obvious cracks in the soil were observed after heating (see the image on the right side of Fig. 7a), implying that steam transport still exhibited a phenomenon of preferential flow. In contrast, when steam was injected after the soil was heated to 60 °C by ERH (Fig. 7b), the middle part reached 100 °C faster than the outlet; meanwhile, the size of cracks in the soil reduced significantly. This trend was improved when the soil was preheated to 70 °C (Fig. 7c), implying that preheating soil could effectively alleviate the problem of preferential flows of steam. Cho et al. reported that the hydraulic conductivity of bentonites increased with increasing soil temperature, the hydraulic conductivity at 80 °C increased up to three times those at 20 °C, and the change in viscosity of water with an increasing temperature significantly contributed to the increase in hydraulic conductivity (Cho et al.,1999). Chen found that heating treatment would produce a large size of pores in boom clay (Chen et al., 2017). Besides, at an elevated temperature, the adsorbed water may degenerate into bulk pore water, and this degeneration results in a higher amount of bulk pore water, increasing permeability because of an increase in flow channel volume (Cho et al., 1999). Therefore, ERH preheating can effectively reduce the resistance of steam transport in soil and improve the convective heat transfer of steam.

3.4 Thermal desorption of PCE from contaminated soil

Fig. 8 compares PCE-spiked soil remediation by ERH alone, SEE alone, and the combined method. As shown in

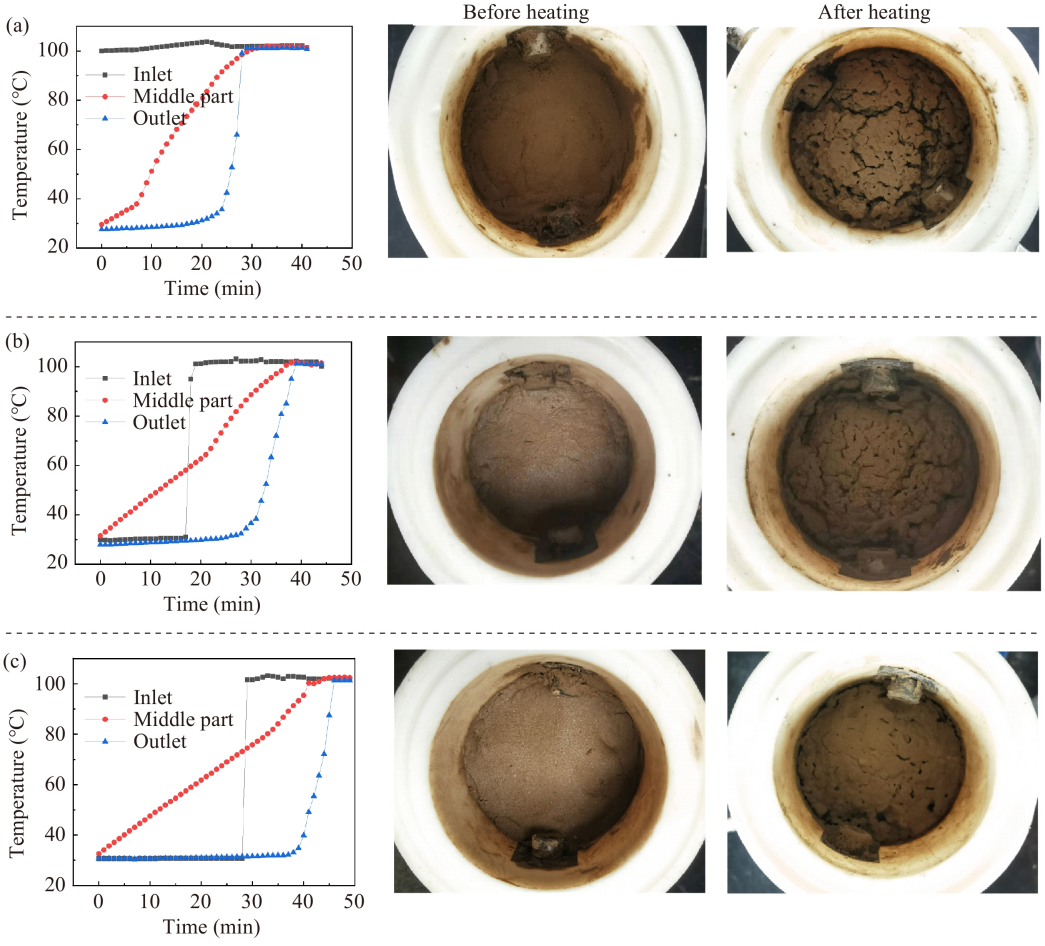

Fig. 7 Profiles of soil temperature and appearances of the top of loam soil samples: (a) heating soil by the combination of ERH and SEE ("SEE+ERH") initialized simultaneously; (b) heating soil by "SEE+ERH" after preheating the soil to 60 °C by ERH; (c) heating soil by "SEE+ERH" after preheating the soil to 70 °C by ERH. Initial soil moisture was set at 20% for all samples. The steam injection was operated at 1 g/min, with an electric field strength of 16 V/cm.

Fig. 8a, for ERH alone operated with an electric field strength of 8 V/cm, the PCE concentration in the off-gas gradually increased with increasing soil temperature. After 100 min, the soil temperature reached 70 °C, and the PCE in the off-gas reached a peak value of 1300 mg/m^3, followed by a fluctuation between 1700 and 650 mg/m^3. After 300 min, the PCE concentration in the off-gas decreased significantly. When 15-mL of water was injected into the soil, the PCE concentration in the off-gas increased again because of the rebound of soil temperature. After 500 min, both temperature and PCE concentration decreased again. Despite the addition of water after 530 min, the PCE concentration no longer increased with increasing temperature, implying that most PCE contaminants had been removed. When the electric field strength was increased to 10 V/cm (see Fig. S5 in SM), both the soil temperature heating rate and the PCE concentration in the off-gas were higher than those at 8 V/cm, with the PCE concentration reaching the maximum value of 2320 mg/m^3 at 100 °C.

Fig. 8b reveals that the soil temperature and the PCE concentration in the off-gas increase rapidly with the continuous steam injection at a 1-g/min rate. After 75 min, the soil temperature reached a peak of 90°C; the PCE concentration reached a peak of 2300 mg/m^3 and began to decrease rapidly after 6 min. When the steam injection rate was reduced to 0.5 g/min, the soil was heated to only 80 °C (see Fig. S6 in SM). The PCE concentration reached a peak of 1460 mg/m^3 at 70 °C. After 320 min, the PCE concentration in the off-gas decreased to 0 mg/m^3. Then, the injection rate increased to 1 g/min. The soil temperature and PCE concentration in the off-gas began to increase again, suggesting that PCE barely desorbed completely at a low steam injection rate.

Fig. 8c shows the operation for the combination of ERH and SEE. First, the soil was preheated to 60 °C by ERH, and the PCE concentration in the off-gas fluctuated at a low level. Afterward, both the soil temperature and the PCE concentration began increasing rapidly when steam was injected into the soil column at a rate of 1 g/min. After 115 min, the soil temperature reached 90 °C, and the PCE concentration in the off-gas reached a peak of 10220 mg/m^3, which was significantly higher than the peak value achieved by ERH alone and SEE alone. Steam was injected at 0.5 g/min until the soil was heated to the boiling point of water, and PCE was almost evacuated completely after 200 min. The experiment with the same ERH condition but a constant steam injection of 0.5 g/min (see Fig. S7 in SM) confirmed the effectiveness of the combined method with an ERH preheating process for PCE extraction.

According to the above results, the thermal desorption efficiency of the combined method is significantly higher than that of SEE and ERH. For SEE, the soil could not be evenly heated when the preferential flow occurred. Steam was expected to flow through more permeable fractures,

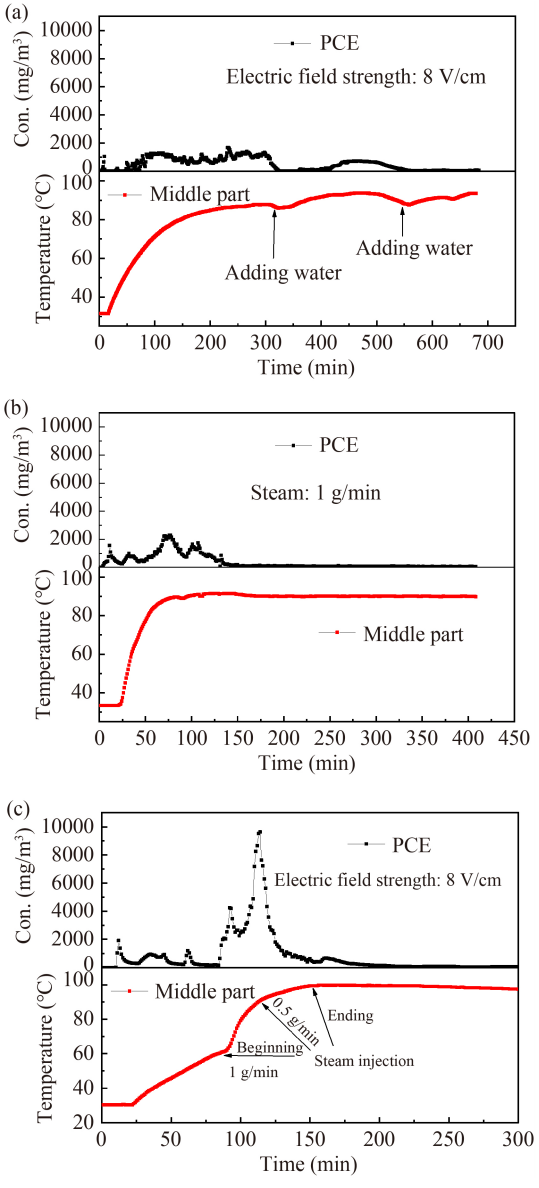

Fig. 8 PCE concentration in off-gas and temperature profiles of loam soil during different remedial processes: (a) ERH treatment, (b) SEE treatment, and (c) ERH + SEE treatment. Initial soil moisture was set at 20% for all samples, with an electric field strength of ERH of 8 V/cm.

rendering it ineffective for displacing contaminants trapped in the porous matrix. For ERH, the evaporation of soil moisture at elevated temperature resulted in the fast attenuation of heating power; meanwhile, it did not have a sweeping effect as that of SEE. The soil heating rate increased significantly for the combined method because of the spatial combination. More importantly, if ERH preheated soil, the improved permeability of soil significantly facilitated steam transport in soil. As a result, the effect of steam stripping and distillation was maximized to remove PCE.

Table 1 shows a detailed comparison of different desorption methods. For all groups, the residual

Table 1 Detailed information about different thermal desorption methods

Method	Electric field strength (V/cm)	Steam rate (g/min)	M_1 (g)	M_2 (g)	Q_s (kW·h)	Q_e (kW·h)	Q/M (kW·h/g)
ERH	8	/	1.11×10^{-1}	5×10^{-4}	/	1.17×10^{-1}	1.05
ERH	10	/	9.19×10^{-2}	1.1×10^{-3}	/	9.1×10^{-2}	0.98
SEE	/	0.5	7.56×10^{-2}	1.91×10^{-2}	1.6×10^{-1}	/	1.69
SEE	/	1	7.61×10^{-2}	1.95×10^{-2}	1.29×10^{-1}	/	1.35
ERH + SEE	8	0.5	9.4×10^{-2}	1.5×10^{-3}	3.01×10^{-2}	4.08×10^{-2}	0.74
ERH + SEE	8	1	1.12×10^{-1}	7×10^{-4}	3.07×10^{-2}	4.11×10^{-2}	0.68

concentrations of PCE in the bottom part of the soil column were all less than 1 mg/kg, and more than 99% removal efficiency was achieved for all methods (see Table S2 in SM). The extracted PCE was distributed into two phases: the effluent gas phase (M_1) and the condensed liquid phase (M_2). Considering the total desorbed PCE, energy consumption per 1-g PCE desorption (Q/M) for all methods could be compared. Comparing ERH alone and SEE alone, ERH is more energy-efficient than SEE because SEE could suffer significant energy loss both from the occurrence of preferential flow and outflow of condensed hot water. Compared with ERH alone (8 V/cm) and SEE alone (1 g/min), the energy consumption of the combined method was reduced by 39.3% and 52.9%, respectively. The energy efficiency of the combined method is significantly higher than that of SEE alone and ERH alone. This observation indicates that the coupling of SEE and ERH should be encouraged for full-scale applications. For example, a steam injection well and ERH electrodes can be integrated into the same heating well. Thus, the cost of building heating wells will be saved, and the energy efficiency for thermal desorption of contaminants can be improved as well. Notably, the energy efficiency of this bench-scale study is lower than that of full-scale site remediation using the combination of SEE and ERH. For remediation engineering at the Young–Rainey STAR Center in the US, a total of 6000-GJ and 4940-GJ energies were delivered to the subsurface via steam injection and ERH, respectively; an estimated total of 1130 kg of volatile organic contaminants was recovered at the energy efficiency of 26.89 kW·h/g (Heron et al, 2005). For the field application of thermal remediation, the complex underground environment resulted in large heat loss, and the difficulty in pollutant desorption increased the heating time as well. This indicates that the coupling of SEE and ERH should be further optimized for full-scale applications to minimize energy consumption.

4 Conclusions

The coupling merits of SEE and ERH were investigated for the first time at a laboratory scale using a laboratory setup. This study proved that soil moisture content, permeability, and steam injection rate influenced the soil temperature rise of the SEE process. Large steam injection pressure, high soil moisture (e.g., > 16.7% for loam), and low soil permeability could lead to preferential steam transport pathways. For the ERH heating process, soil electrical conductivity and the evaporation of pore water significantly affected the heating power. When the two methods were combined, the temperature rise rate of soil was significantly accelerated. Steam injection heated soil and reduced soil electrical resistivity, thereby improving ERH heating efficiency. Meanwhile, the preheating of soil by ERH could increase soil permeability and alleviate the problem of preferential flow of SEE, which is favorable to the heat conduction of steam. These coupling merits enabled the combined method to be significantly more energy-efficient than SEE or ERH alone for soil remediation, even though the coupling did not broaden the temperature range for thermal desorption. The combined method is expected to save desorption energy for full-scale applications and reduce the construction cost of heating wells because of the compact structure after spatial coupling.

Acknowledgements This study was supported by the National Key R&D Program of China (No. 2019YFC1805700).

Electronic Supplementary Material Supplementary material is available in the online version of this article at https://doi.org/10.1007/s11783-022-1582-z and is accessible for authorized users.

References

Archie G E (1942). The electrical resistivity log as an aid in determining some reservoir characteristics. Transactions of the AIME, 146(1): 54–62

Arps J J (1953). The effect of temperature on the density and electrical resistivity of sodium chloride solutions. Journal of Petroleum Technology, 5(10): 17–20

Brouwers H J H, Gilding B H (2006). Steam stripping of the unsaturated zone of contaminated sub-soils: the effect of diffusion/dispersion in the start-up phase. Journal of Contaminant Hydrology, 83(1−2): 1–26

Cai J, Wei W, Hu X, Wood D A (2017). Electrical conductivity models in saturated porous media: A review. Earth-Science Reviews, 171:

419–433

Carrigan C R, Nitao J J (2000). Predictive and diagnostic simulation of *in situ* electrical heating in contaminated, low-permeability soils. Environmental Science & Technology, 34(22): 4835–4841

Chen W Z, Ma Y S, Yu H D, Li F F, Li X L, Sillen X (2017). Effects of temperature and thermally-induced microstructure change on hydraulic conductivity of Boom Clay. Journal of Rock Mechanics and Geotechnical Engineering, 9(3): 383–395

Cho W J, Lee J O, Chun K S (1999). The temperature effects on hydraulic conductivity of compacted bentonite. Applied Clay Science, 14(1−3): 47–58

Davis E L (1998). Steam Injection for Soil and Aquifer remediation. US. Environmental Protection Agency

Ding D, Song X, Wei C, LaChance J (2019). A review on the sustainability of thermal treatment for contaminated soils. Environmental Pollution, 253: 449–463

USEPA (2004). *In Situ* Thermal Treatment of Chlorinated Solvents: Fundamentals and Field Applications, EPA 542-R-04–010. Washington, DC: Office of Solid Waste and Emergency Response

Fournier R, Thibodeau M, French C T (2009). Measurement of steam generator or reactor vessel moisture carryover using a non-radioactive chemical tracer, International Conference on Nuclear Engineering, 459–467

Geng Z, Liu B, Li G, Zhang F (2021). Enhancing DNAPL removal from low permeability zone using electrical resistance heating with pulsed direct current. Journal of Hazardous Materials, 413: 125455

Han Z, Jiao W, Tian Y, Hu J, Han D (2020). Lab-scale removal of PAHs in contaminated soil using electrical resistance heating: Removal efficiency and alteration of soil properties. Chemosphere, 239: 124496

Heron G, Carroll S, Nielsen S G (2005). Full-scale removal of DNAPL constituents using steam-enhanced extraction and electrical resistance heating. Ground Water Monitoring and Remediation, 25(4): 92–107

Heron G, Van Zutphen M, Christensen T H, Enfield C G (1998). Soil heating for enhanced remediation of chlorinated solvents: A laboratory study on resistive heating and vapor extraction in a silty, low-permeable soil contaminated with trichloroethylene. Environmental Science & Technology, 32(10): 1474–1481

Horst J, Munholland J, Hegele P, Klemmer M, Gattenby J (2021). *In situ* thermal remediation for source areas: technology advances and a review of the market From 1988–2020. Ground Water Monitoring and Remediation, 41(1): 17–31

Kaslusky S F, Udell K S (2005). Co-injection of air and steam for the prevention of the downward migration of DNAPLs during steam enhanced extraction: an experimental evaluation of optimum injection ratio predictions. Journal of Contaminant Hydrology, 77(4): 325–347

Triplett Kingston J L, Dahlen P R, Johnson P C (2010). State-of-the-practice review of *in situ* thermal technologies. Ground Water Monitoring and Remediation, 30(4): 64–72

Li J, Wang L, Peng L, Deng Y, Deng D (2020). A combo system consisting of simultaneous persulfate recirculation and alternating current electrical resistance heating for the implementation of heat activated persulfate ISCO. Chemical Engineering Journal, 385: 123803

Martin E J, Kueper B H (2011). Observation of trapped gas during electrical resistance heating of trichloroethylene under passive venting conditions. Journal of Contaminant Hydrology, 126(3−4): 291–300

Martin E J, Mumford K G, Kueper B H (2016). Electrical resistance heating of Clay layers in water-saturated sand. Ground Water Monitoring and Remediation, 36(1): 54–61

Munholland J (2015). Electrical Resistance Heating of Groundwater Impacted by Chlorinated Solvents in Heterogeneous Sand [Diss]

Munholland J L, Mumford K G, Kueper B H (2016). Factors affecting gas migration and contaminant redistribution in heterogeneous porous media subject to electrical resistance heating. Journal of Contaminant Hydrology, 184: 14–24

Newmark R L, Aines R D (1995). Summary of the LLNL Gasoline Spill Demonstration-Dynamic Underground Stripping Project. Lawrence Livermore National Laboratory

Peng S, Wang N, Chen J (2013). Steam and air co-injection in removing residual TCE in unsaturated layered sandy porous media. Journal of Contaminant Hydrology, 153: 24–36

Piquemal J (1994). Saturated steam relative permeabilities of unconsolidated porous media. Transport porous. El Medico, 17(2): 105–120

Sleep B E, McClure P D (2001). Removal of volatile and semivolatile organic contamination from soil by air and steam flushing. Journal of Contaminant Hydrology, 50(1−2): 21–40

Stephenson K M, Novakowski K, Davis E, Heron G (2006). Hydraulic characterization for steam enhanced remediation conducted in fractured rock. Journal of Contaminant Hydrology, 82(3-4): 220–240

Trine L S D, Davis E L, Roper C, Truong L, Tanguay R L, Simonich S L M (2019). Formation of PAH derivatives and increased developmental toxicity during steam enhanced extraction remediation of creosote contaminated Superfund soil. Environmental Science & Technology, 53(8): 4460–4469

Tse K K C, Lo S L, Wang J W H (2001). Pilot study of in-situ thermal treatment for the remediation of pentachlorophenol-contaminated aquifers. Environmental Science & Technology, 35(24): 4910–4915

Tzovolou D N, Aggelopoulos C A, Theodoropoulou M A, Tsakiroglou C D (2011). Remediation of the unsaturated zone of NAPL-polluted low permeability soils with steam injection: An experimental study. Journal of Soils and Sediments, 11(1): 72–81

Zhang T, Lowry G V, Capiro N L, Chen J, Chen W, Chen Y, Dionysiou D D, Elliott D W, Ghoshal S, Hofmann T, et al. (2019). *In situ* remediation of subsurface contamination: Opportunities and challenges for nanotechnology and advanced materials. Environmental Science. Nano, 6(5): 1283–1302